

Designing dynamically corrected gates robust to multiple noise sources using geometric space curvesHunter T. Nelson,^{*} Evangelos Piliouras,^{*} Kyle Connelly, and Edwin Barnes[†]*Department of Physics, Virginia Tech, Blacksburg, Virginia 24061, USA
and Virginia Tech Center for Quantum Information Science and Engineering, Blacksburg, Virginia 24061, USA*

(Received 7 December 2022; accepted 2 June 2023; published 7 July 2023)

Noise-induced gate errors remain one of the main obstacles to realizing a broad range of quantum information technologies. Dynamical error suppression using carefully designed control schemes is critical for overcoming this challenge. Such schemes must be able to correct against multiple noise sources simultaneously afflicting a qubit to reach error-correction thresholds. Here we present a general framework for designing control fields that simultaneously suppress both noise in the fields themselves as well as transverse dephasing noise. Using the recently developed space curve quantum control formalism, in which robust quantum evolution is mapped to closed geometric curves in a multidimensional Euclidean space, we derive the minimal conditions necessary to guarantee the simultaneous cancellation of both types of noise to leading order. In particular, we find that the cancellation of control field noise requires the derivative of the space curve to have zero-area projections, which is a much more subtle property compared to the closed-curve condition needed to suppress transverse dephasing. We present several techniques for solving both these conditions simultaneously and provide explicit examples of error-resistant control fields. Our work also sheds light on the relation between holonomic evolution and the suppression of control field errors.

DOI: [10.1103/PhysRevA.108.012407](https://doi.org/10.1103/PhysRevA.108.012407)**I. INTRODUCTION**

Quantum information technologies require control schemes that satisfy both reachability and robustness criteria. Reachability refers to the set of achievable unitary evolutions under a given control scheme [1], while robustness refers to noise insensitivity, which is critical for reaching quantum error-correction thresholds [2]. In recent years, the field of quantum optimal control has put forward several techniques for implementing a desired target evolution or logical gate operation while maintaining a certain level of noise robustness, including both analytical and numerical methods [3–26]. While purely numerical approaches have been shown to be quite powerful in many contexts, with their convergence typically guaranteed, supplementing these with analytical information about the control landscape can further boost performance and potentially lead to globally optimal solutions.

Holonomic quantum computation [27–36] is one example of an analytical technique that was proposed to design robust control schemes. In this approach, gates are realized via the accumulation of geometric phases under holonomic evolution. Since such phases depend only on geometric properties of the path traversed in Hilbert space, and not on the rate of traversal, the resulting gates should be insensitive to noise that leaves the path invariant [37,38]. Evidence of such robustness against certain types of control field noise has been shown in both theoretical [39–47] and experimental work [48–51].

However, whether or not these methods really provided robustness to noise across a broad range of practical settings has been a matter of contention, and several explicit examples of holonomic gates that did not exhibit the desired robustness were known [31,38,39,52–57]. It was later found in Ref. [58] that, for a large class of holonomic gates, it is possible to construct an equivalent nonholonomic gate with the same noise sensitivity, suggesting that even when robustness was achieved, holonomy may not be the underlying cause. On the other hand, it was shown in Ref. [59] that, under certain conditions, single-qubit gates that were simultaneously robust to multiplicative control field noise and transverse dephasing noise were necessarily holonomic.

Another analytical approach to building noise-robust gates is through the space curve quantum Control (SCQC) formalism [57,60–64]. This method makes use of geometric space curves to design gates that are robust to transverse dephasing noise. Because this method provides access to the entire solution space of robust pulses, it offers the highest possible degree of flexibility in finding control waveforms that conform to experimental requirements. Most importantly, this approach does not rely on a conjecture, robustness is guaranteed by construction. However, so far SCQC has only been applied to transverse dephasing noise, while in most qubit platforms, including quantum dot spin qubits [65–69], superconducting transmons [70–72], and trapped ions [73,74], control field noise is of comparable importance. The authors of Ref. [75] took a first step in addressing this issue by showing how to incorporate holonomy into the SCQC formalism, yielding holonomic gates with guaranteed insensitivity to transverse noise. However, this approach is still susceptible to the usual uncertainties regarding whether holonomic

^{*}These authors contributed equally.[†]efbarnes@vt.edu

evolution is robust to control field errors, leaving open the question of whether it is possible to guarantee the simultaneous cancellation of both transverse dephasing errors and control field errors in quantum gates.

In this work, we extend the SCQC formalism to construct single-qubit gates that are simultaneously robust to both transverse dephasing noise and multiplicative control field noise. SCQC has not previously been applied to control field noise due primarily to the subtle way in which it appears within the formalism. We do this in the context of a quasistatic noise model that is widely applicable across multiple qubit platforms and show how to use this method to obtain waveforms that generate the desired noise-robust logic gates. Suitable control waveforms are obtained by designing space curves that satisfy certain constraints and then computing their curvatures. We show that, in addition to being closed, which guarantees the cancellation of transverse noise errors, the derivative of the curve must also satisfy a zero-area condition to ensure multiplicative control field errors are also suppressed. We prove that these conditions are both necessary and sufficient in that any robust pulse will be associated with curves satisfying these conditions. Unlike prior works on dynamically corrected gates [11,76–78], we make no assumptions about the pulse waveforms that are used and our gate designs are based on single, continuous pulses. We also give several methods for constructing explicit examples of curves obeying these criteria and we present a mathematical theorem that allows one to easily check whether a given curve derivative integrates to a closed curve. Additionally, we demonstrate how the freedom to switch between the dynamical and geometric phase without changing the robustness of gates, as first discussed in Refs. [58,59], manifests in the SCQC formalism. This, in turn, sheds light on the relation between holonomic evolution and the cancellation of control field errors.

The paper is organized as follows. In Sec. II we utilize the SCQC formalism to derive space-curve conditions that facilitate the construction of gates simultaneously robust to transverse noise and multiplicative control field noise. We also compare and contrast these conditions with the parallel transport condition associated with holonomic evolution. In Sec. III we discuss general methods for constructing space curves that yield noise-robust gates and compare the performance of gates generated using this approach. It is here that we also present a theorem that allows one to check if a given tangent curve produces a corresponding closed curve. We conclude in Sec. IV.

II. NOISE-CANCELLATION CONDITIONS, SPACE CURVES, AND RELATION TO HOLONOMIC EVOLUTION

In this section, we consider a general single-qubit Hamiltonian simultaneously subject to two types of noise, one additive, the other multiplicative. Although the SCQC formalism is extended to include the cancellation of time-dependent noise [63], in this work we focus solely on the case of quasistatic noise, which is pervasive in solid-state qubits, where control timescales are fast compared to noise fluctuations [79–82]. Since, in most, qubit platforms, the bulk of the noise is concentrated at low frequencies, the quasistatic model is already sufficient for designing high-fidelity control schemes.

While further refinements can be achieved by accounting for noise coloration, we leave this to future work. Here, our goal is to derive conditions on space curves that guarantee the simultaneous cancellation of both types of quasistatic noise. In this section, we also examine the connection between these noise-cancellation conditions and the conditions that define holonomic evolution.

A. Noise-cancellation conditions

We begin with a three-field control Hamiltonian of the form

$$H_0(t) = \frac{\Omega(t)}{2} [\cos \Phi(t) \sigma_x + \sin \Phi(t) \sigma_y] + \frac{\Delta(t)}{2} \sigma_z, \quad (1)$$

where we refer to $\Omega(t)$, $\Phi(t)$, $\Delta(t)$ as the driving, phase, and detuning fields, respectively, and σ_x , σ_y , σ_z are Pauli matrices. We consider multiplicative errors in $\Omega(t)$ and additive errors in $\Delta(t)$:

$$\Omega(t) \rightarrow (1 + \epsilon)\Omega(t), \quad (2)$$

$$\Delta(t) \rightarrow \Delta(t) + \delta_z, \quad (3)$$

where ϵ and δ_z are unknown, stochastic noise parameters that are assumed to be small and constant during the evolution. This model captures the common situation in which noise causes a slow, random rescaling of the driving field, as occurs for instance in exchange pulses in quantum dot spin qubits subject to charge noise [79]. Additive fluctuations in $\Delta(t)$ are a widely used model of dephasing noise in qubit energy levels, where the dephasing time T_2^* is set by the width of the distribution from which δ_z is sampled [81]. Both types of noise are non-Markovian (both in experiments and in our model), and here we make no assumptions about whether these fluctuations obey Gaussian or non-Gaussian statistics. Although in experiments, it is known that the noise carries a nontrivial time dependence, the quasistatic model considered here serves as a good approximation in most cases since the bulk of the noise is typically concentrated at low frequencies [79,81,83–86]. In particular, the noise usually has a $1/f$ type spectrum. Pulses that cancel quasistatic noise will thus cancel the majority of the colored noise seen in experiments. The SCQC formalism has also been extended to the case of time-dependent transverse noise in Ref. [63], where it was shown that pulses that suppress such noise correspond to sequences of closed space curves.

To quantify the deviation away from the ideal evolution caused by ϵ and δ_z , it helps to switch to the interaction picture defined by $U_0(t)$, the evolution operator generated by $H_0(t)$. The Magnus expansion [87] of the interaction picture evolution operator is then controlled by the small parameters ϵ and δ_z . At first order we have

$$U_I(t) \approx e^{-i\Pi_1(t)}, \quad (4)$$

with

$$\begin{aligned} \Pi_1(t) = & \int_0^t dt' H_I(t') = \frac{\delta_z}{2} \int_0^t dt' U_0^\dagger(t') \sigma_z U_0(t') \\ & + \frac{\epsilon}{2} \int_0^t dt' U_0^\dagger(t') \Omega(t') \\ & \times [\cos \Phi(t') \sigma_x + \sin \Phi(t') \sigma_y] U_0(t'). \end{aligned} \quad (5)$$

Following Ref. [60], we interpret the term proportional to δ_z as a curve in three-dimensional (3D) Euclidean space that we refer to as the “space curve” or “error curve” $\vec{r}(t)$:

$$\vec{r}(t) \cdot \vec{\sigma} \equiv \int_0^t dt' U_0^\dagger(t') \sigma_z U_0(t'). \quad (6)$$

By construction, it then follows that canceling transverse dephasing noise to first order in δ_z corresponds to ensuring that $\vec{r}(t)$ is a closed curve. To study these 3D space curves, we define an orthonormal frame called the Frenet-Serret frame [88], consisting of the tangent vector $\vec{T} \equiv \dot{\vec{r}}$, the normal vector $\vec{N} \equiv \vec{T} / \|\vec{T}\|$, and the binormal vector $\vec{B} \equiv \vec{T} \times \vec{N}$. (Note that throughout this work \vec{T} denotes a tangent vector, while T denotes a gate time.) These vectors then satisfy the Frenet-Serret equations

$$\begin{aligned} \dot{\vec{T}} &= \kappa \vec{N}, \\ \dot{\vec{N}} &= -\kappa \vec{T} + \tau \vec{B}, \\ \dot{\vec{B}} &= -\tau \vec{N}. \end{aligned} \quad (7)$$

The functions κ and τ are the curvature and torsion of the curve, and via the Frenet-Serret equations they uniquely determine the curve up to rigid rotations in an interval where $\kappa \neq 0$ (see Appendix A). Once we find a closed space curve, we can find the corresponding control fields Ω , Φ , and Δ from the curvature κ and torsion τ of the space curve

$$\kappa = \Omega, \quad (8)$$

$$\tau = \dot{\Phi} - \Delta. \quad (9)$$

We see that any closed space curve yields control fields that generate a quantum evolution that is insensitive to quasistatic transverse dephasing errors. Note also that Φ and Δ are not uniquely determined by the geometry of the space curve.

The second term in Eq. (5) can also be written in terms of the space curve. From the definition of the space curve in Eq. (6) we see that

$$\begin{aligned} \dot{\vec{T}}(t) \cdot \vec{\sigma} &= \frac{d}{dt} (U_0^\dagger \sigma_z U_0) \\ &= iU_0^\dagger [H_0, \sigma_z] U_0 \\ &= -2i(U_0^\dagger \sigma_z U_0) U_0^\dagger \begin{pmatrix} 0 & \frac{\Omega(t)}{2} e^{-i\Phi(t)} \\ \frac{\Omega(t)}{2} e^{i\Phi(t)} & 0 \end{pmatrix} U_0 \\ &= -2i(\vec{T}(t) \cdot \vec{\sigma}) U_0^\dagger \begin{pmatrix} 0 & \frac{\Omega(t)}{2} e^{-i\Phi(t)} \\ \frac{\Omega(t)}{2} e^{i\Phi(t)} & 0 \end{pmatrix} U_0, \end{aligned} \quad (10)$$

which implies that

$$\begin{aligned} \Omega(t) U_0^\dagger(t) [\cos \Phi(t) \sigma_x + \sin \Phi(t) \sigma_y] U_0(t) \\ &= i(\vec{T}(t) \cdot \vec{\sigma})(\vec{T}(t) \cdot \vec{\sigma}) \\ &= -(\vec{T}(t) \times \dot{\vec{T}}(t)) \cdot \vec{\sigma}. \end{aligned} \quad (11)$$

Thus, we see that the leading-order errors from both types of noise can be expressed in terms of the tangent curve $\vec{T}(t)$, with

Eq. (5) becoming

$$\Pi_1(t) = \frac{\vec{\sigma}}{2} \cdot \int_0^t dt' (-\epsilon \vec{T} \times \dot{\vec{T}} + \delta_z \vec{T}). \quad (12)$$

A doubly robust qubit evolution [$U_I(T) \approx \mathbb{1}$] then requires that the following two conditions be simultaneously satisfied:

$$\int_0^T dt \vec{T} = 0, \quad (13)$$

$$\int_0^T dt (\vec{T} \times \dot{\vec{T}}) = 0. \quad (14)$$

The second condition is proportional to the area swept out by the projection of the tangent vector onto each plane. (Interestingly, it was found in Ref. [60] that if the same condition is satisfied by the error curve itself, the dephasing error is suppressed to second order.) Therefore, to cancel both types of error to first order, we must find a closed space curve \vec{r} whose tangent vector \vec{T} sweeps out zero area when projected onto any plane.

B. Relation to the holonomic evolution

Much of the previous work on designing robust quantum gates focused on making the evolution holonomic, meaning that the dynamical phase vanishes at the final gate time [37,38,75]. Here, we express the dynamical phase in terms of the tangent vector \vec{T} , and by comparing this to the noise-cancellation conditions Eqs. (13) and (14), we show that holonomic evolution is neither necessary nor sufficient to guarantee robust evolution.

The dynamical phase is given by [89]

$$\begin{aligned} \alpha_d(t) &= \int_0^t \langle \psi(t') | H_0(t') | \psi(t') \rangle dt' \\ &= \int_0^t \langle \psi(0) | U_0^\dagger(t') H_0(t') U_0(t') | \psi(0) \rangle dt'. \end{aligned} \quad (15)$$

Defining the initial Pauli vector as $\vec{P}(0) = \langle \psi(0) | \vec{\sigma} | \psi(0) \rangle$ and using Eq. (11), the dynamical phase may then be written as

$$\begin{aligned} \alpha_d(t) &= \frac{1}{2} \int_0^t \langle \psi(0) | (-\vec{T} \times \dot{\vec{T}} + \Delta(t') \vec{T}) \cdot \vec{\sigma} | \psi(0) \rangle \\ &= \frac{\vec{P}(0)}{2} \cdot \int_0^t (-\vec{T} \times \dot{\vec{T}} + \Delta(t') \vec{T}) dt'. \end{aligned} \quad (16)$$

Despite the striking resemblance to Eq. (12), canceling the dynamical phase does not necessarily lead to error robustness. To elaborate on this, we first observe from Eq. (16) that the dynamical phase involves a projection of the integral onto the Pauli vector of the initial state. Making this vanish requires either a special choice of the detuning field $\Delta(t)$ or a carefully designed tangent vector \vec{T} to ensure the integral in Eq. (16) is orthogonal to $\vec{P}(0)$ at the final time. Another approach one can take is to impose the parallel transport condition, which is tantamount to requiring that the integrand in Eq. (16) is orthogonal to $\vec{P}(0)$ at all times [75]. Regardless of which approach is taken to make $\alpha_d(T)$ vanish, it does not necessarily follow that Eqs. (13) and (14) are satisfied. Therefore, the condition that the evolution be holonomic does not guarantee that either type of noise is canceled.

Conversely, it also holds that a robust evolution does not necessarily have to be holonomic. To see this, consider taking a holonomic evolution $U(t)$ and forming a new evolution $\tilde{U}(t) = Z_{\Lambda(t)}U(t)Z_{-\Lambda(0)}$, where $Z_{\Lambda(t)} = e^{-i\frac{\Lambda(t)}{2}\sigma_z}$ and $\Lambda(t)$ is an arbitrary differentiable function. This new evolution has the initial condition $\tilde{U}(0) = \mathbb{1}$ and evolves under the effective Hamiltonian

$$\begin{aligned} \tilde{H} &\equiv i\dot{\tilde{U}}\tilde{U}^\dagger = Z_\Lambda H Z_\Lambda^\dagger + i\left(\frac{d}{dt}Z_\Lambda\right)Z_\Lambda^\dagger \\ &= \frac{\Omega}{2}(\cos\tilde{\Phi}\sigma_x + \sin\tilde{\Phi}\sigma_y) + \frac{\tilde{\Delta}}{2}\sigma_z, \end{aligned} \quad (17)$$

where $\tilde{\Phi} \equiv \Phi + \Lambda$, $\tilde{\Delta} \equiv \Delta + \dot{\Lambda}$. Therefore, changing the driving fields from $\{\Phi, \Delta\} \rightarrow \{\tilde{\Phi}, \tilde{\Delta}\}$ will implement the gate \tilde{U} rather than U . Changing the control fields in this way leaves the curvature and torsion $\tau = \dot{\Phi} - \Delta$ invariant, and thus \vec{r} can only differ from \bar{r} by a rigid rotation. However, since the error Hamiltonian can be written as $H_I = \frac{1}{2}(-\epsilon\vec{T} \times \dot{\vec{T}} + \delta_z\vec{T}) \cdot \vec{\sigma}$, changing the phase and detuning fields in this way can only change \tilde{H}_I and \tilde{U}_I by a constant rotation and so such a change does not affect the robustness of the evolution to any order. This does, however, change the dynamical phase since $\Lambda(t)$, and hence $\tilde{\Delta}(t)$, can be chosen arbitrarily. A similar observation was made by the authors of Ref. [58] using the filter function formalism. Additionally, we note here that $\tilde{U}(T)$ does not have to be equal to $U(T)$. By properly choosing $\Lambda(T)$ and $\Lambda(0)$, we can add arbitrary z rotations before and after a robust gate without affecting its robustness.

One exception to the above analysis occurs in the case of a constant detuning field Δ , where robustness to both types of noise does imply that the evolution is holonomic, as first pointed out in Ref. [59]. This is readily seen from the SCQC formalism by observing that, if a space curve satisfies Eqs. (13) and (14), then from Eq. (16) it immediately follows that $\alpha_d(T) = 0$. Note, however, that the dynamical phase is only guaranteed to vanish if Δ is constant. Transformations Z_Λ that change the detuning field from one constant value to another, i.e., ones for which $\Lambda(t)$ is linear in t , will preserve the holonomic condition.

III. CONSTRUCTION OF DOUBLY ROBUST EVOLUTIONS

We now proceed to construct several classes of curves satisfying the conditions given in Eqs. (13) and (14). These conditions ensure that the driving pulses produced from these curves are doubly robust to first-order multiplicative driving field noise and additive transverse dephasing noise. We present three different methods for constructing curves that satisfy these conditions. The first method utilizes an ansatz consisting of even and odd parity space curve components comprised of trigonometric functions with frequencies fixed such that both robustness conditions are satisfied. We refer to such curves as ‘‘parity curves.’’ The second method accomplishes the cancellation of errors by instead utilizing an ansatz for the tangent curve for which Eq. (14) is enforced by symmetry. Choosing parameters equal to Bessel function roots guarantees closure of the space curve so that Eq. (13) is also satisfied, yielding ‘‘Bessel curves.’’ The third method consists of constructing the tangent curve on a sphere such

that it traces out ‘‘tilted circles’’ that sweep zero area while also containing the origin in its convex hull. We prove that the later condition ensures the corresponding space curve is closed, and so both Eqs. (13) and (14) are again satisfied.

For each example curve presented below, we confirm the robustness of the resulting gate by numerically simulating the evolution in the presence of both types of errors and computing the gate infidelity \mathcal{I} using the definition introduced in Ref. [90] (see also Ref. [75])

$$\mathcal{F} = \frac{1}{6}\text{Tr}(U_n^\dagger U_n) + \frac{1}{6}|\text{Tr}(U_t^\dagger U_n)|^2. \quad (18)$$

A. Parity curves

First, we consider the approach that utilizes the parity and periodicity of trigonometric functions. This class of curves can be written in the form

$$\vec{r}(\lambda) = f_x(\omega_x\lambda)\hat{x} + f_y(\omega_y\lambda)\hat{y} + f_z(\omega_z\lambda)\hat{z}, \quad (19)$$

where each function $f_i(\omega_i\lambda)$ is periodic with period $2\pi/\omega_i$ and either even or odd in λ . Parameterizations of this sort make it straightforward to impose symmetries in the space curve, and this in turn can make it easier to satisfy the noise-cancellation conditions. In particular, curves whose components are all odd or all even functions satisfy these conditions. These ‘‘parity curves’’ are related to the trigonometric curves considered in the literature on the differential geometry of curves [91]. The periodicity of such functions guarantees the curve is closed, provided we choose all the ratios of the frequencies to be rational numbers so that a least common multiple always exists. The parity property of the trigonometric functions ensures the curves have vanishing projected areas for both the space and tangent curves. For instance, if we start with a curve whose components are of the even type, then \vec{r} will be comprised of odd functions and \vec{r} will be comprised of even functions. Therefore, the integral of the cross product Eq. (14) will only contain odd functions and will, therefore, vanish over the period of the curve.

The following is an example of a parity curve, where we choose each component to be odd:

$$\vec{r}(\lambda) = \sin(\lambda/2)\hat{x} + \sin(\lambda)\cos^2(\lambda)\hat{y} + \sin(\lambda)\cos(\lambda)\hat{z}. \quad (20)$$

Here, $\lambda \in [0, 4\pi]$. Before we can extract a pulse from this curve, we must first switch to the arc-length parametrization t defined by $\|\frac{d}{dt}\vec{r}[\lambda(t)]\|^2 = 1$ and such that $t \in [0, T]$, where $\lambda(T) = 4\pi$. It follows immediately that $\vec{r}(T) = \vec{r}[\lambda(T)] = 0$, and because of the built-in parity symmetry, the corresponding tangent curve $\vec{T}(t) = \dot{\vec{r}}(t)$ satisfies Eq. (14), implying that both types of noise are canceled. In fact, this curve also has vanishing projected areas $\int_0^T dt \vec{r}(t) \times \vec{T}(t) = 0$, so transverse dephasing noise is actually canceled up to second order in this example. The control fields obtained from the curvature and torsion of $\vec{r}(t)$ using Eq. (9) are shown in Fig. 1.

To demonstrate the improved performance of the gate generated by this curve, we compare its infidelity is not satisfied. These three curves have the following tangent

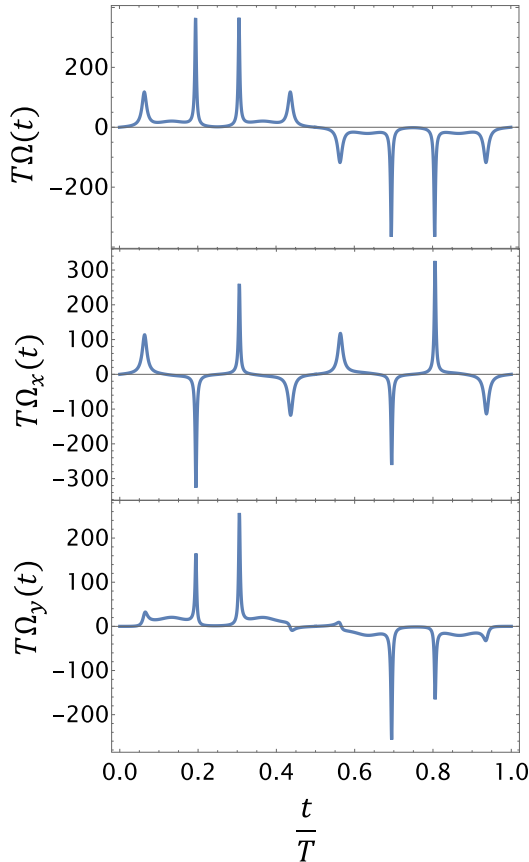


FIG. 1. Control fields that generate an identity gate robust to both control field noise and transverse dephasing noise obtained using the parity curve given in Eq. (20). Here, $\Omega_x = \Omega \cos \Phi$, $\Omega_y = \Omega \sin \Phi$, $\Delta = 0$, and T is the gate time.

curves:

$$\dot{\vec{r}}(t) = \sin(t) \cos(t) \hat{x} + \sin^2(t) \hat{y} + \cos(t) \hat{z}, \quad (21)$$

$$\begin{aligned} \dot{\vec{r}}(t) = & \frac{1}{4}(\sqrt{2} \cos(2t) - 2 \cos(t)) \hat{x} - \frac{1}{4}(\sqrt{2} \sin(2t) \\ & + 2 \sin(t)) \hat{y} + \frac{1}{2} \sqrt{\sqrt{2} \cos(3t) + \frac{5}{2}} \hat{z}, \end{aligned} \quad (22)$$

$$\dot{\vec{r}}(t) = \sin(t) \cos(2t) \hat{x} + \sin(t) \sin(2t) \hat{y} + \cos(t) \hat{z}, \quad (23)$$

where $t \in [0, 2\pi]$ and we set $T = 1$ to simplify the notation. Here Eq. (21) is a nonrobust curve that breaks both conditions (13) and (14), Eq. (22) has a vanishing area but generates a nonclosed curve, and Eq. (23) does not sweep zero area but does generate a closed curve. The space curves obtained by integrating these tangent curves are shown in Figs. 2(a) to 2(c). We also note that Eq. (22), which is built using the technique given in Ref. [92], is a less trivial example of a tangent curve with vanishing area that does not use the parity property built into Eq. (20). The fully robust curve of Eq. (20) is shown in Fig. 2(d). All four of these curves produce identity gates.

The gate infidelities corresponding to all four of the above curves are shown in Fig. 2 as a function of the strengths of both types of noise. Figure 2(a) clearly shows the reduction in performance that results when the space curve

breaks both conditions, Eqs. (13) and (14), with the infidelity growing rapidly as both noise strengths are increased. However, Figs. 2(b) and 2(c) both exhibit a clear robustness against one type of noise depending on which noise-cancellation condition is satisfied. Finally, Fig. 2(d) shows a marked improvement in suppressing both types of noise, where now both noise-cancellation conditions are satisfied. The infidelity in this case in fact scales better than the expected ϵ^2 , $(T\delta_z)^2$ scaling. The improved scaling in $T\delta_z$ can be understood from the fact that the projected areas of the space curve all vanish, as noted above. The ϵ scaling suggests that the ϵ^2 term in the Magnus expansion also vanishes for this example; this in turn may be a consequence of the parity symmetry. Further investigation of the higher-order terms of the Magnus expansion would be needed to confirm this. Finally, we note that, although the use of parity curves makes it easy to satisfy both noise-cancellation constraints at the same time, the control fields in this example as shown in Fig. 1 may be hard to implement in practice due to their sharp (although nonsingular) features. Bandwidth constraints can still be enforced by either rescaling the gate time T (and hence the pulse amplitudes) or by restricting the frequency parameters in Eq. (19) appropriately. However, both approaches may lead to longer than necessary gate times. In the subsequent sections, we present two other methods of constructing curves that satisfy both noise-cancellation constraints while also yielding more experimentally friendly pulse shapes.

B. Bessel curves

Our second technique for constructing curves that satisfy Eqs. (13) and (14) starts by defining the following ansatz for the normalized tangent curve:

$$\vec{T}[\theta(t)] = [\cos(q\theta) \sin \theta, \sin(q\theta) \sin \theta, \cos \theta], \quad (24)$$

where q is a proportionality constant between the azimuthal and polar angles. This formulation provides a curve that is already expressed in its own arc-length parametrization and which is solely controlled by a function $\theta(t)$. This ansatz makes the pulse error constraint particularly simple:

$$\int_0^T dt (\vec{T} \times \dot{\vec{T}}) = \int_{\theta(0)}^{\theta(T)} d\theta \left(\vec{T} \times \frac{\partial \vec{T}}{\partial \theta} \right) = 0, \quad (25)$$

where examination of the third component forces us to require

$$\theta(0) = \theta(T). \quad (26)$$

This one boundary constraint is equivalent to the vanishing area condition, Eq. (14), along all three projections. For the curve to be closed, we additionally need three real integrals to vanish. These integrals come from plugging Eq. (24) into Eq. (13). However, to simplify the process of finding suitable functions $\theta(t)$, we will upgrade these to three complex integral constraints

$$\int_0^T e^{i\theta(t)} dt = 0, \quad (27)$$

$$\int_0^T e^{i\theta(t)(1 \pm q)} dt = 0, \quad (28)$$

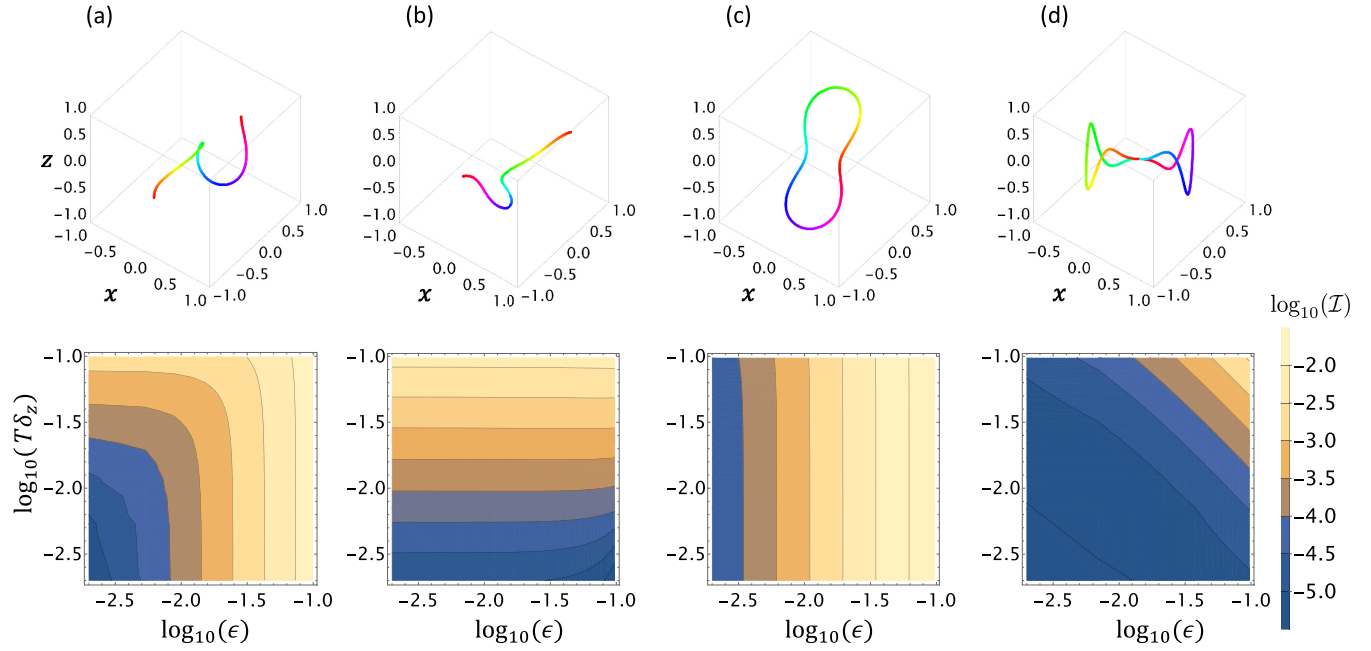


FIG. 2. Four space curves (top row) that correspond to identity gates and the corresponding gate infidelities \mathcal{I} (bottom row) as a function of control field noise (ϵ) and transverse dephasing noise (δ_z). (a) The space curve defined in Eq. (21) which does not satisfy either of the noise-cancellation constraints, Eqs. (13) and (14). (b) The space curve defined in Eq. (22) which satisfies Eq. (14) but not Eq. (13). (c) The space curve defined in Eq. (23) which satisfies Eq. (13) but not Eq. (14). (d) The doubly robust “parity” space curve defined in Eq. (20) which satisfies both Eqs. (13) and (14).

where Eq. (28) should be understood as two separate constraints, one for each choice of the sign in front of q . Although Eqs. (27) and (28) are generally stronger constraints than Eq. (13), these complex constraints have the advantage that they can be solved approximately using Bessel functions, as we explain in more detail below.

We note in passing that if we choose $q = 0$, then Eq. (28) becomes redundant, and the one independent integral constraint that remains, Eq. (27), coincides with the closed-curve constraint for plane curves [62]. This is to be expected since setting $q = 0$ in Eq. (24) restricts the tangent curve, and hence the space curve, to the xz plane. In this case, $\dot{\theta}(t)$ can be interpreted as the curvature of the plane curve [64] and Eq. (13) is equivalent to Eq. (27). The zero-area constraint on the tangent curve, Eq. (14), remains equivalent to Eq. (26).

For any other value of $q \neq 0$, Eq. (28) imposes an independent constraint on the space curve. The magnitude of the curvature of the space curve is given by

$$|\kappa(t)| = \sqrt{q^2 \sin^2[\theta(t)] + 1} |\dot{\theta}(t)|. \quad (29)$$

We see that if we impose $\dot{\theta}(0) = 0 = \dot{\theta}(T)$, the resulting pulse envelope $\Omega(t) = \kappa(t)$ will start and end at zero as should be the case for a smooth pulse. This condition and Eq. (26) are both satisfied by the following ansatz:

$$\theta(t) = x_i \cos\left(\frac{2\pi}{T}t\right), \quad (30)$$

where x_i is a real constant. We refer to the space curve obtained from this choice of $\theta(t)$ as a “Bessel curve.” Inserting this ansatz into Eqs. (27) and (28) and comparing the results to the integral representation of the Bessel function of the

first kind [93], we see that all the space curve constraints are satisfied by choosing x_i and $(1 \pm q)x_i$ to be Bessel function zeros

$$J_0(x_i) = 0, \quad (31)$$

$$J_0[(1 \pm q)x_i] = 0. \quad (32)$$

In the case of a plane curve ($q = 0$), the resulting evolution generated by the sinusoidal $\Omega(t)$ is robust to pulse errors since Eq. (26) holds; more surprisingly, we see that there exist particular pulse amplitudes x_i for which dephasing noise is also suppressed. For more general values of $q \neq 0$, we have a 3D space curve, and we must choose q so that both $(1 + q)x_i$ and $(1 - q)x_i$ are also Bessel function zeros. Although we cannot, in general, find values of q for which these quantities are both exact zeros, we can make them approximate zeros by finding a q that minimizes $[(1 - q)x_i - x_{i-1}]^2 + [(1 + q)x_i - x_{i+1}]^2$. For three consecutive exact Bessel zeros x_{i-1} , x_i , x_{i+1} , this function is minimized when

$$q = \frac{x_{i+1} - x_{i-1}}{2x_i}. \quad (33)$$

The parameters x_i and q together give us discrete control over the smoothness of the space curve, and hence, the bandwidth of the resulting control field. The curve and associated control fields for the choice $x_i = 5.5201$, $q = 0.5660$ are shown in Figs. 3(a) and 3(b), respectively. In Fig. 3(c), we confirm the expected insensitivity of the resulting z gates to both transverse dephasing noise and multiplicative control field noise. Different z rotations are constructed by adjusting the gauge choice for Φ and Δ as discussed in the previous section. Figure 3(d) shows that this robustness persists across all

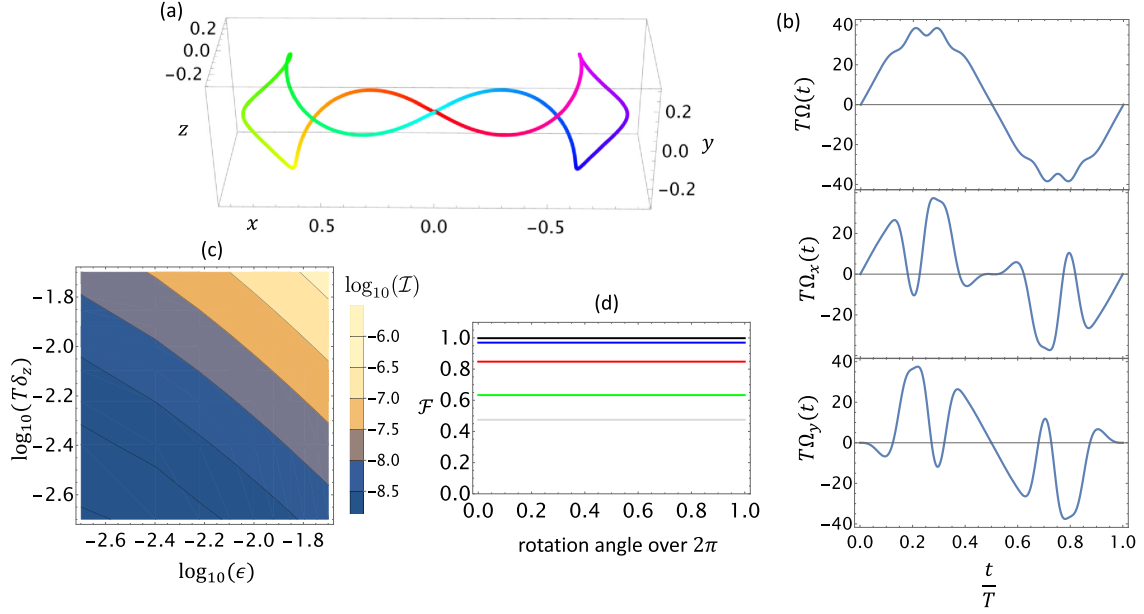


FIG. 3. (a) The “Bessel curve” obtained from Eqs. (24) and (30) with $x_i = 5.5201$, $q = 0.5660$. (b) Control fields that implement a doubly robust identity gate obtained from the curvature and torsion of the Bessel curve in (a). Here $\Omega_x = \Omega \cos \Phi$, $\Omega_y = \Omega \sin \Phi$, $\Delta = 0$, and T is the gate time. (c) The infidelity of z rotations as a function of the strengths of transverse dephasing noise (δ_z) and multiplicative driving field noise (ϵ). The infidelity for each value of δ_z and ϵ is averaged over the uniform distribution $[0, 2\pi]$ of z -rotation angles. (d) The fidelity \mathcal{F} versus z -rotation angle (divided by 2π). Each line corresponds to different values of ϵ and δ_z (both have the same value along each line). Starting from the top, the error values are $\delta_z, \epsilon = 0, 0.1, 0.2, 0.3$, and 0.4 , respectively.

possible z rotations. It is noteworthy that in this example, the particular space curve also happens to have vanishing projected areas, and so therefore second-order dephasing errors are also suppressed.

C. Tilted circles

Another very general strategy for constructing curves that satisfy the robustness conditions comes from the observation that the integral giving the area swept out by the tangent curve is independent of the parametrization of that curve

$$\int_0^T \vec{T} \times \dot{\vec{T}} dt = \int \vec{T} \times d\vec{T}. \quad (34)$$

Thus we can start by drawing a tangent curve that sweeps out zero area and then try to find a parametrization such that the space curve is closed. Let s be the arc length of \vec{T} , i.e., $\|d\vec{T}/ds\| = 1$. Then after designing a tangent curve $\vec{T}(s)$ that sweeps out to zero area, we must find a parametrization $s(t)$ that gives a closed space curve upon integrating $\vec{T}[s(t)] \equiv \vec{T}(t)$.

The curvature κ and torsion τ of \vec{r} are related to $\vec{T}(t)$ as follows:

$$\kappa = \|\dot{\vec{T}}\| = \frac{ds}{dt}, \quad (35)$$

$$\begin{aligned} \tau &= -\vec{N} \cdot \dot{\vec{B}} = -\vec{N} \cdot \frac{d}{dt}(\vec{T} \times \vec{N}) = -\frac{1}{\kappa} \dot{\vec{T}} \cdot \frac{d}{dt} \left(\vec{T} \times \frac{1}{\kappa} \dot{\vec{T}} \right) \\ &= -\frac{1}{\kappa} \frac{d}{dt} \vec{T} \cdot \vec{T} \times \kappa \left(\frac{1}{\kappa} \frac{d}{dt} \right)^2 \vec{T} = \kappa \vec{T} \cdot \frac{d\vec{T}}{ds} \times \frac{d^2\vec{T}}{ds^2}. \end{aligned} \quad (36)$$

The vector triple product above is the geodesic curvature of the tangent curve $\kappa_{g,T}$, so this relationship can be written as $\tau/\kappa = \kappa_{g,T}$.

Not every tangent curve can be reparameterized to give a closed space curve, however. For instance, in Eq. (22) the z component of \vec{T} is always positive and so the z component of \vec{r} will be nondecreasing regardless of how \vec{T} is parameterized. Fortunately, we find a simple visual criterion that can be used to determine if a given \vec{T} curve can yield a closed space curve.

Theorem 1. A tangent curve $\vec{T}(s)$ can generate a closed space curve if and only if the convex hull of $\vec{T}(s)$ contains the origin.

A more precise statement of this theorem and its proof can be found in Appendix B. We also note that this theorem has appeared before in the mathematical literature [94].

We now use this general method to find a family of pulses yielding x rotations X_θ , which when combined with virtual z rotations and/or phase ramping can give any single-qubit gate. The pulses in Fig. 4(c) are derived from tangent curves comprised of “tilted circles,” as shown in Figs. 4(a) and 4(b). The curve goes from $\vec{T}_0 = [\cos(\theta/2), 0, \sin(\theta/2)]^T$ to $\vec{T}_f = [\cos(-\theta/2), 0, \sin(-\theta/2)]^T$ along a great circle arc. However, it goes around two smaller circles before and after to cancel the area swept out by the great circle arc. The upper and lower circles are normal to the vectors $\hat{n}_0 = (0, -\sin \alpha, \cos \alpha)^T$ and $\hat{n}_f = (0, -\sin \alpha, -\cos \alpha)^T$, respectively. The sign of the normal vectors are chosen so that the area contribution from the circle points along \hat{n} :

$$\vec{A}_{\text{circle}} = \pi r_{\text{circle}}^2 \hat{n} = \pi \sin^2 \gamma \hat{n}, \quad (37)$$

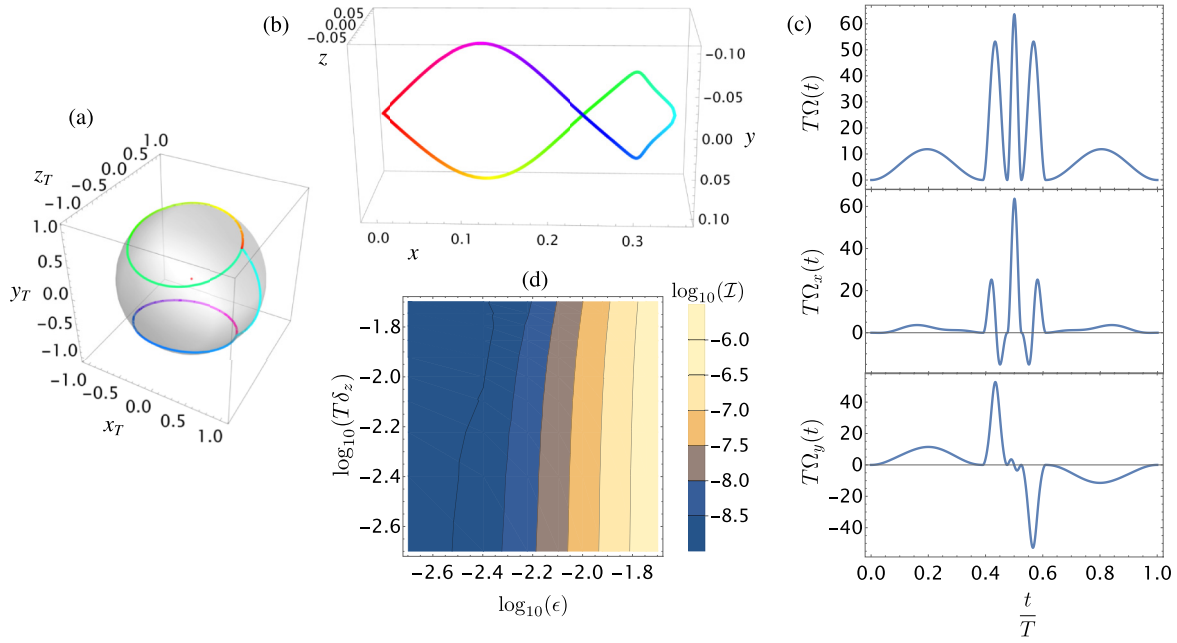


FIG. 4. (a) The “tilted circles” tangent curve, shown here for $\theta = \pi/2$. The hue of the curve indicates the manner in which it is traced. We also show the origin (in red) to show that it is contained in the convex hull of this curve. (b) A closed space curve generated from the tilted circle tangent curve in (a). The hue of this curve matches that of the tangent curve and shows the speed at which different sections of the tangent curve are traversed. (c) Control fields for a doubly robust $R(\frac{\pi}{2}X)$ gate extracted from the curvature and torsion of the curve in (b). To achieve the desired z -rotation angle, a constant detuning field is chosen appropriately. (d) Infidelity of the tilted curve-based $R(\frac{\pi}{2}X)$ gate versus transverse dephasing noise strength (δ_z) and multiplicative driving field noise strength (ϵ).

where γ is defined as the angle between \vec{T}_0 and \hat{n}_0 (and the angle between \vec{T}_f and \hat{n}_f):

$$\cos \gamma = \vec{T}_0 \cdot \hat{n}_0 = \vec{T}_f \cdot \hat{n}_f = \sin \frac{\theta}{2} \cos \alpha. \quad (38)$$

The area contribution of the arc from \vec{T}_0 to \vec{T}_f is $\vec{A}_{\text{arc}} = \theta/2 \hat{y}$, and the total area swept out is

$$\begin{aligned} \vec{A} &= \frac{\theta}{2} \hat{y} + \pi \sin^2 \gamma (\hat{n}_0 + \hat{n}_f) \\ &= \left[\frac{\theta}{2} - 2\pi \sin \alpha \left(1 - \sin^2 \left(\frac{\theta}{2} \right) \cos^2 \alpha \right) \right] \hat{y}. \end{aligned} \quad (39)$$

To cancel driving error, we require $\vec{A} = 0$, which gives an implicit equation defining $\alpha(\theta)$: $2\pi \sin \alpha (1 - \sin^2(\theta/2) \cos^2 \alpha) = \theta/2$. We also see that the origin is contained in the convex hull of this curve and so it can be reparameterized to give a closed space curve. In Fig. 4, we validate the inclusion of the origin in the convex hull of the tangent curve and present the infidelity of the resulting evolution. The area of low infidelity is the largest among all our results, which emphasizes the fact that the degree of error-cancellation affects the rate at which the quality of the gate degrades with increasing noise strength and not its absolute fidelity.

IV. CONCLUSION

In conclusion, we presented the description of the geometric control in the language of the (SCQC) formalism defined in the error interaction picture. Utilizing the Magnus expansion,

we can transfer the noise suppression problem entirely to a geometric space curve where each order of error is associated with a respective geometric property. Specifically, a zero total area of the tangent curve leads to cancellation of first-order multiplicative error and a closed curve reduces the contribution of a static error. The relationship to the dynamical phase is subsequently revealed and manifests the fact that its cancellation does not necessarily imply total tolerance to (first-order) errors in the driving field. The validation of our theoretical results are supported by simulation of three types of curves: Trigonometric “parity curves,” “Bessel curves,” and the “tilted circles” approach, which are curves satisfying both geometric conditions. Analysis of the infidelity plots revealed the significantly greater performance of such gates compared to gates that did not satisfy either robustness condition. Mediated by the gauge freedom provided by the torsion, any desired phase accumulation did not degrade the level of robustness of this geometric scheme.

ACKNOWLEDGMENTS

This work is supported by the Office of Naval Research (Grant No. N00014-21-1-2629), the Army Research Office (Grant No. W911NF-17-0287), and the Department of Energy (Grant No. DE-SC0022389).

APPENDIX A: SIGNED CURVATURE AND INFLECTION POINTS

The introduction of the moving frame allows us to uniquely map the control fields to the Frenet-Serret vectors, in an

interval free of inflection points, essentially $\kappa(t) \neq 0$. In general, Eq. (9) implicitly assumes the differentiability of $\Omega(t)$, despite the fact that $\dot{\Omega}(t)$ does not appear explicitly. When inflection points (points where the curvature vanishes) arise, the curvature function contains cusps at these points; therefore, a gauge transformation allows us to use a generalized version of the curvature which changes sign at every inflection point in the interval of evolution, ensuring the continuity of the normal vector [95]. If t_i^* are points of zero curvature, then the driving field is given by

$$\Omega(t) = \kappa(t) \sum_{i=1}^N (-1)^i \theta(t - t_i) \theta(t_{i+1} - t). \quad (\text{A1})$$

Essentially, this is a form of signed curvature. Similarly, the phase field exhibits a π discontinuity at such points, yielding the same behavior for the fields along σ_x and σ_y . The same technique was introduced in the context of the SCQC formalism in Ref. [57].

APPENDIX B: CONVEX HULL THEOREM

Here we give a more precise statement and proof of Theorem 1 from the main text.

Theorem 2. A tangent curve $\vec{T}(s)$ can generate a closed space curve if and only if the convex hull of $\vec{T}(s)$ contains the origin. Additionally, in order for $\kappa(t)$ to be finite at all times

(no delta function pulses), the origin must be in the interior of the convex hull of $\vec{T}(s)$.

The convex hull of $\vec{T}(s)$ is the set of vectors

$$\mathcal{C} = \left\{ \int_0^{s_f} ds \lambda(s) \vec{T}(s) : \lambda(s) \geq 0, \int_0^{s_f} ds \lambda(s) = 1 \right\}. \quad (\text{B1})$$

Given some particular parametrization $s(t)$, we can write $\vec{R}(T)$ as

$$\begin{aligned} \vec{R}(T) &= \int_0^T dt \vec{T}(t) = \int_0^S ds \frac{dt}{ds} \vec{T}(s) \\ &= T \left(\int_0^S ds \frac{1}{T\kappa(s)} \vec{T}(s) \right), \end{aligned} \quad (\text{B2})$$

where $S \equiv s(T)$. We can therefore identify $\vec{R}(T)/T$ as a point in \mathcal{C} , with $\lambda(s) = 1/T\kappa(s)$; clearly, $1/T\kappa \geq 0$ since $\kappa \geq 0$, and

$$\int_0^S ds \frac{1}{T\kappa(s)} = \frac{1}{T} \int_0^S ds \frac{dt}{ds} = \frac{1}{T} \int_0^T dt = 1. \quad (\text{B3})$$

Thus in order for the space curve to be closed, i.e., $\vec{R}(T) = 0$, there must be some choice of $\lambda(s) = 1/T\kappa(s)$ such that $\int_0^{s_f} ds \lambda(s) \vec{T}(s) = 0$, i.e., the origin must be in the convex hull of \vec{T} .

Additionally, if κ is finite at all times, then $\lambda(s) = 1/T\kappa(s) > 0$. The points in \mathcal{C} with $\lambda(s) > 0$ for all s are points in the interior of \mathcal{C} .

-
- [1] D. D'Alessandro, *Introduction to Quantum Control and Dynamics* (Chapman and Hall/CRC, Boca Raton, 2021).
- [2] H. K. Ng, D. A. Lidar, and J. Preskill, Combining dynamical decoupling with fault-tolerant quantum computation, *Phys. Rev. A* **84**, 012305 (2011).
- [3] M. J. Biercuk, H. Uys, A. P. VanDevender, N. Shiga, W. M. Itano, and J. J. Bollinger, Optimized dynamical decoupling in a model quantum memory, *Nature (London)* **458**, 996 (2009).
- [4] K. Khodjasteh, H. Bluhm, and L. Viola, Automated synthesis of dynamically corrected quantum gates, *Phys. Rev. A* **86**, 042329 (2012).
- [5] G. H. Low, T. J. Yoder, and I. L. Chuang, Optimal arbitrarily accurate composite pulse sequences, *Phys. Rev. A* **89**, 022341 (2014).
- [6] J. T. Merrill and K. R. Brown, [Progress in compensating pulse sequences for quantum computation](#), in *Quantum Information and Computation for Chemistry* (2014), pp. 241–294.
- [7] K. R. Brown, A. W. Harrow, and I. L. Chuang, Arbitrarily accurate composite pulse sequences, *Phys. Rev. A* **70**, 052318 (2004).
- [8] T. van der Sar, Z. H. Wang, M. S. Blok, H. Bernien, T. H. Taminiau, D. M. Toyli, D. A. Lidar, D. D. Awschalom, R. Hanson, and V. V. Dobrovitski, Decoherence-protected quantum gates for a hybrid solid-state spin register, *Nature (London)* **484**, 82 (2012).
- [9] K. Khodjasteh and D. A. Lidar, Fault-Tolerant Quantum Dynamical Decoupling, *Phys. Rev. Lett.* **95**, 180501 (2005).
- [10] T. J. Green, J. Sastrawan, H. Uys, and M. J. Biercuk, Arbitrary quantum control of qubits in the presence of universal noise, *New J. Phys.* **15**, 095004 (2013).
- [11] K. Khodjasteh and L. Viola, Dynamically Error-Corrected Gates for Universal Quantum Computation, *Phys. Rev. Lett.* **102**, 080501 (2009).
- [12] L. Viola and E. Knill, Robust Dynamical Decoupling of Quantum Systems with Bounded Controls, *Phys. Rev. Lett.* **90**, 037901 (2003).
- [13] K. Khodjasteh, D. A. Lidar, and L. Viola, Arbitrarily Accurate Dynamical Control in Open Quantum Systems, *Phys. Rev. Lett.* **104**, 090501 (2010).
- [14] W. Zhang, N. P. Konstantinidis, V. V. Dobrovitski, B. N. Harmon, L. F. Santos, and L. Viola, Long-time electron spin storage via dynamical suppression of hyperfine-induced decoherence in a quantum dot, *Phys. Rev. B* **77**, 125336 (2008).
- [15] L. Viola and S. Lloyd, Dynamical suppression of decoherence in two-state quantum systems, *Phys. Rev. A* **58**, 2733 (1998).
- [16] C. Brif, R. Chakrabarti, and H. Rabitz, Control of quantum phenomena: Past, present and future, *New J. Phys.* **12**, 075008 (2010).
- [17] C. P. Koch, Controlling open quantum systems: Tools, achievements, and limitations, *J. Phys.: Condens. Matter* **28**, 213001 (2016).
- [18] M. Y. Niu, S. Boixo, V. N. Smelyanskiy, and H. Neven, Universal quantum control through deep reinforcement learning, *npj Quantum Inf.* **5**, 33 (2019).
- [19] L. Giannelli, P. Sgroi, J. Brown, G. S. Paroanu, M. Paternostro, E. Paladino, and G. Falci, A tutorial on optimal control and reinforcement learning methods for quantum technologies, *Phys. Lett. A* **434**, 128054 (2022).
- [20] C. P. Koch, U. Boscain, T. Calarco, G. Dirr, S. Filipp, S. J. Glaser, R. Kosloff, S. Montangero, T. Schulte-Herbrüggen,

- D. Sugny, and F. K. Wilhelm, Quantum optimal control in quantum technologies. strategic report on current status, visions and goals for research in europe, *EPJ Quantum Technol.* **9**, 19 (2022).
- [21] L. Van Damme, D. Sugny, and S. J. Glaser, Application of the small-tip-angle approximation in the toggling frame for the design of analytic robust pulses in quantum control, *Phys. Rev. A* **104**, 042226 (2021).
- [22] Q. Ansel, S. J. Glaser, and D. Sugny, Selective and robust time-optimal rotations of spin systems, *J. Phys. A: Math. Theor.* **54**, 085204 (2021).
- [23] N. Khaneja, T. Reiss, C. Kehlet, T. Schulte-Herbrüggen, and S. J. Glaser, Optimal control of coupled spin dynamics: Design of NMR pulse sequences by gradient ascent algorithms, *J. Magn. Reson.* **172**, 296 (2005).
- [24] M. M. Müller, R. S. Said, F. Jelezko, T. Calarco, and S. Montangero, One decade of quantum optimal control in the chopped random basis, *Rep. Prog. Phys.* **85**, 076001 (2022).
- [25] C. Kabytayev, T. J. Green, K. Khodjasteh, M. J. Biercuk, L. Viola, and K. R. Brown, Robustness of composite pulses to time-dependent control noise, *Phys. Rev. A* **90**, 012316 (2014).
- [26] K. Khodjasteh and L. Viola, Dynamical quantum error correction of unitary operations with bounded controls, *Phys. Rev. A* **80**, 032314 (2009).
- [27] L.-J. Guo, H. Xu, Z.-Y. Fang, T. Chen, K. Wei, and C. Zhang, Optimizing nonadiabatic geometric quantum gates against off-resonance error by dynamical correction in a silicon-based spin qubit, *Phys. Rev. A* **107**, 012604 (2023).
- [28] P. Zanardi and M. Rasetti, Holonomic quantum computation, *Phys. Lett. A* **264**, 94 (1999).
- [29] F. Wilczek and A. Zee, Appearance of Gauge Structure in Simple Dynamical Systems, *Phys. Rev. Lett.* **52**, 2111 (1984).
- [30] M. V. Berry, Transitionless quantum driving, *J. Phys. A: Math. Theor.* **42**, 365303 (2009).
- [31] P. Solinas, P. Zanardi, and N. Zanghì, Robustness of non-abelian holonomic quantum gates against parametric noise, *Phys. Rev. A* **70**, 042316 (2004).
- [32] E. Sjöqvist, Geometric phases in quantum information, *Int. J. Quantum Chem.* **115**, 1311 (2015).
- [33] E. Sjöqvist, V. Azimi Mousolou, and C. M. Canali, Conceptual aspects of geometric quantum computation, *Quant. Info. Proc.* **15**, 3995 (2016).
- [34] G. F. Xu, J. Zhang, D. M. Tong, E. Sjöqvist, and L. C. Kwek, Nonadiabatic Holonomic Quantum Computation in Decoherence-Free Subspaces, *Phys. Rev. Lett.* **109**, 170501 (2012).
- [35] U. Güngördü, Y. Wan, and M. Nakahara, Non-adiabatic universal holonomic quantum gates based on abelian holonomies, *J. Phys. Soc. Jpn.* **83**, 034001 (2014).
- [36] Z. Chen, Observable-geometric phases and quantum computation, *Int. J. Theor. Phys.* **59**, 1255 (2020).
- [37] G. De Chiara and G. M. Palma, Berry Phase for a Spin 1/2 Particle in a Classical Fluctuating Field, *Phys. Rev. Lett.* **91**, 090404 (2003).
- [38] S.-L. Zhu and P. Zanardi, Geometric quantum gates that are robust against stochastic control errors, *Phys. Rev. A* **72**, 020301(R) (2005).
- [39] A. Carollo, I. Fuentes-Guridi, M. F. Santos, and V. Vedral, Geometric Phase in Open Systems, *Phys. Rev. Lett.* **90**, 160402 (2003).
- [40] G. De Chiara and G. M. Palma, A geometric analysis of the effects of noise on berry phase, *Int. J. Theor. Phys.* **47**, 2165 (2008).
- [41] Z. S. Wang, C. Wu, X.-L. Feng, L. C. Kwek, C. H. Lai, C. H. Oh, and V. Vedral, Nonadiabatic geometric quantum computation, *Phys. Rev. A* **76**, 044303 (2007).
- [42] J. T. Thomas, M. Lababidi, and M. Tian, Robustness of single-qubit geometric gate against systematic error, *Phys. Rev. A* **84**, 042335 (2011).
- [43] Z.-T. Liang, X. Yue, Q. Lv, Y.-X. Du, W. Huang, H. Yan, and S.-L. Zhu, Proposal for implementing universal superadiabatic geometric quantum gates in nitrogen-vacancy centers, *Phys. Rev. A* **93**, 040305(R) (2016).
- [44] T. Chen and Z.-Y. Xue, Nonadiabatic Geometric Quantum Computation with Parametrically Tunable Coupling, *Phys. Rev. Appl.* **10**, 054051 (2018).
- [45] B.-J. Liu, X.-K. Song, Z.-Y. Xue, X. Wang, and M.-H. Yung, Plug-and-Play Approach to Nonadiabatic Geometric Quantum Gates, *Phys. Rev. Lett.* **123**, 100501 (2019).
- [46] T. Chen and Z.-Y. Xue, High-Fidelity and Robust Geometric Quantum Gates that Outperform Dynamical Ones, *Phys. Rev. Appl.* **14**, 064009 (2020).
- [47] J. Pachos and P. Zanardi, Quantum holonomies for quantum computing, *Int. J. Mod. Phys. B* **15**, 1257 (2001).
- [48] S. Berger, M. Pechal, A. A. Abdumalikov, Jr., C. Eichler, L. Steffen, A. Fedorov, A. Wallraff, and S. Filipp, Exploring the effect of noise on the berry phase, *Phys. Rev. A* **87**, 060303(R) (2013).
- [49] B. B. Zhou, P. C. Jerger, V. O. Shkolnikov, F. J. Heremans, G. Burkard, and D. D. Awschalom, Holonomic Quantum Control by Coherent Optical Excitation in Diamond, *Phys. Rev. Lett.* **119**, 140503 (2017).
- [50] F. Kleibler, A. Lazarev, and S. Arroyo-Camejo, Universal, high-fidelity quantum gates based on superadiabatic, geometric phases on a solid-state spin-qubit at room temperature, *npj Quantum Inf.* **4**, 49 (2018).
- [51] Y. Xu, Z. Hua, T. Chen, X. Pan, X. Li, J. Han, W. Cai, Y. Ma, H. Wang, Y. P. Song, Z.-Y. Xue, and L. Sun, Experimental Implementation of Universal Nonadiabatic Geometric Quantum Gates in a Superconducting Circuit, *Phys. Rev. Lett.* **124**, 230503 (2020).
- [52] A. Nazir, T. P. Spiller, and W. J. Munro, Decoherence of geometric phase gates, *Phys. Rev. A* **65**, 042303 (2002).
- [53] A. Blais and A.-M. S. Tremblay, Effect of noise on geometric logic gates for quantum computation, *Phys. Rev. A* **67**, 012308 (2003).
- [54] J. Dajka and J. Łuczka, Bifurcations of the geometric phase of a qubit asymmetrically coupled to the environment, *J. Phys. A: Math. Theor.* **41**, 442001 (2008).
- [55] Y. Ota and Y. Kondo, Composite pulses in NMR as nonadiabatic geometric quantum gates, *Phys. Rev. A* **80**, 024302 (2009).
- [56] E. Sjöqvist, D.-M. Tong, L. M. Andersson, B. Hessmo, M. Johansson, and K. Singh, Non-adiabatic holonomic quantum computation, *New J. Phys.* **14**, 103035 (2012).
- [57] F. Zhuang, J. Zeng, S. E. Economou, and E. Barnes, Noise-resistant landau-zener sweeps from geometrical curves, *Quantum* **6**, 639 (2022).
- [58] R. K. L. Colmenar, U. Güngördü, and J. P. Kestner, Conditions for equivalent noise sensitivity of geometric and dynamical quantum gates, *PRX Quantum* **3**, 030310 (2022).

- [59] R. K. L. Colmenar and J. P. Kestner, Reverse engineering of one-qubit filter functions with dynamical invariants, *Phys. Rev. A* **106**, 032611 (2022).
- [60] J. Zeng, C. H. Yang, A. S. Dzurak, and E. Barnes, Geometric formalism for constructing arbitrary single-qubit dynamically corrected gates, *Phys. Rev. A* **99**, 052321 (2019).
- [61] D. Buterakos, S. Das Sarma, and E. Barnes, Geometrical formalism for dynamically corrected gates in multiqubit systems, *PRX Quantum* **2**, 010341 (2021).
- [62] J. Zeng, X.-H. Deng, A. Russo, and E. Barnes, General solution to inhomogeneous dephasing and smooth pulse dynamical decoupling, *New J. Phys.* **20**, 033011 (2018).
- [63] B. Li, F. A. Calderon-Vargas, J. Zeng, and E. Barnes, Designing arbitrary single-axis rotations robust against perpendicular time-dependent noise, *New J. Phys.* **23**, 093032 (2021).
- [64] E. Barnes, F. A. Calderon-Vargas, W. Dong, B. Li, J. Zeng, and F. Zhuang, Dynamically corrected gates from geometric space curves, *Quantum Sci. Technol.* **7**, 023001 (2022).
- [65] S. M. Arif, A. Bera, A. Ghosh, and M. Ghosh, Exploring noise-effect on the intraband transition lifetime of impurity doped quantum dots, *Biointerface Res. Appl. Chem.* **11**, 8639 (2021).
- [66] N. E. Penthorn, J. S. Schoenfield, J. D. Rooney, L. F. Edge, and H. Jiang, Two-axis quantum control of a fast valley qubit in silicon, *npj Quantum Inf.* **5**, 94 (2019).
- [67] E. J. Connors, J. Nelson, L. F. Edge, and J. M. Nichol, Charge-noise spectroscopy of Si/SiGe quantum dots via dynamically-decoupled exchange oscillations, *Nat. Commun.* **13**, 940 (2022).
- [68] D. Culcer, A. L. Saraiva, B. Koiller, X. Hu, and S. Das Sarma, Valley-Based Noise-Resistant Quantum Computation Using Si Quantum Dots, *Phys. Rev. Lett.* **108**, 126804 (2012).
- [69] X. Mi, S. Kohler, and J. R. Petta, Landau-zener interferometry of valley-orbit states in Si/SiGe double quantum dots, *Phys. Rev. B* **98**, 161404(R) (2018).
- [70] J. A. Valery, S. Chowdhury, G. Jones, and N. Didier, Dynamical sweet spot engineering via two-tone flux modulation of superconducting qubits, *PRX Quantum* **3**, 020337 (2022).
- [71] A. A. Houck, J. Koch, M. H. Devoret, S. M. Girvin, and R. J. Schoelkopf, Life after charge noise: Recent results with transmon qubits, *Quant. Info. Proc.* **8**, 105 (2009).
- [72] M. B. Metcalfe, E. Boaknin, V. Manucharyan, R. Vijay, I. Siddiqi, C. Rigetti, L. Frunzio, R. J. Schoelkopf, and M. H. Devoret, Measuring the decoherence of a qantronium qubit with the cavity bifurcation amplifier, *Phys. Rev. B* **76**, 174516 (2007).
- [73] I. Talukdar, D. J. Gorman, N. Daniilidis, P. Schindler, S. Ebadi, H. Kaufmann, T. Zhang, and H. Häffner, Implications of surface noise for the motional coherence of trapped ions, *Phys. Rev. A* **93**, 043415 (2016).
- [74] Q. A. Turchette, C. J. Myatt, B. E. King, C. A. Sackett, D. Kielpinski, W. M. Itano, C. Monroe, and D. J. Wineland, Decoherence and decay of motional quantum states of a trapped atom coupled to engineered reservoirs, *Phys. Rev. A* **62**, 053807 (2000).
- [75] W. Dong, F. Zhuang, S. E. Economou, and E. Barnes, Doubly geometric quantum control, *PRX Quantum* **2**, 030333 (2021).
- [76] X. Wang *et al.*, Composite pulses for robust universal control of singlet-triplet qubits, *Nat. Commun.* **3**, 997 (2012).
- [77] J. P. Kestner *et al.*, Noise-Resistant Control for a Spin Qubit Array, *Phys. Rev. Lett.* **110**, 140502 (2013).
- [78] X. Wang *et al.*, Robust quantum gates for singlet-triplet spin qubits using composite pulses, *Phys. Rev. A* **89**, 022310 (2014).
- [79] O. E. Dial, M. D. Shulman, S. P. Harvey, H. Bluhm, V. Umansky, and A. Yacoby, Charge Noise Spectroscopy Using Coherent Exchange Oscillations in a Singlet-Triplet Qubit, *Phys. Rev. Lett.* **110**, 146804 (2013).
- [80] P. J. J. O'Malley, J. Kelly, R. Barends, B. Campbell, Y. Chen, Z. Chen, B. Chiaro, A. Dunsworth, A. G. Fowler, I.-C. Hoi, E. Jeffrey, A. Megrant, J. Mutus, C. Neill, C. Quintana, P. Roushan, D. Sank, A. Vainsencher, J. Wenner, T. C. White, A. N. Korotkov, A. N. Cleland, and J. M. Martinis, Qubit Metrology of Ultralow Phase Noise Using Randomized Benchmarking, *Phys. Rev. Appl.* **3**, 044009 (2015).
- [81] F. Martins, F. K. Malinowski, P. D. Nissen, E. Barnes, S. Fallahi, G. C. Gardner, M. J. Manfra, C. M. Marcus, and F. Kuemmeth, Noise Suppression Using Symmetric Exchange Gates in Spin Qubits, *Phys. Rev. Lett.* **116**, 116801 (2016).
- [82] M. D. Hutchings, J. B. Hertzberg, Y. Liu, N. T. Bronn, G. A. Keefe, M. Brink, J. M. Chow, and B. L. T. Plourde, Tunable Superconducting Qubits with Flux-Independent Coherence, *Phys. Rev. Appl.* **8**, 044003 (2017).
- [83] P. Krantz *et al.*, A quantum engineer's guide to superconducting qubits, *Appl. Phys. Rev.* **6**, 021318 (2019).
- [84] J. Bylander *et al.*, Noise spectroscopy through dynamical decoupling with a superconducting flux qubit, *Nat. Phys.* **7**, 565 (2011).
- [85] P. V. Klimov *et al.*, Fluctuations of Energy-Relaxation Times in Superconducting Qubits, *Phys. Rev. Lett.* **121**, 090502 (2018).
- [86] J. J. Burnett *et al.*, Decoherence benchmarking of superconducting qubits, *npj Quantum Inf.* **5**, 54 (2019).
- [87] S. Blanes, F. Casas, J. Oteo, and J. Ros, The magnus expansion and some of its applications, *Phys. Rep.* **470**, 151 (2009).
- [88] A. Pressley, *Elementary Differential Geometry* (Springer, London, 2010).
- [89] Y. Aharonov and J. Anandan, Phase Change During a Cyclic Quantum Evolution, *Phys. Rev. Lett.* **58**, 1593 (1987).
- [90] L. H. Pedersen, N. M. Møller, and K. Mølmer, Fidelity of quantum operations, *Phys. Lett. A* **367**, 47 (2007).
- [91] Y. Animov, *Differential Geometry and Topology of Curves* (CRC Press, Boca Raton, FL, 2001).
- [92] J. L. Weiner, Closed curves of constant torsion. II, *Proc. Am. Math. Soc.* **67**, 306 (1977).
- [93] J. D. Jackson, *Classical Electrodynamics*, 3rd ed. (Wiley, New York, 1999).
- [94] W. Fenchel, On the differential geometry of closed space curves, *Bull. Amer. Math. Soc.* **57**, 44 (1951).
- [95] S. Hu, M. Lundgren, and A. J. Niemi, Discrete frenet frame, inflection point solitons, and curve visualization with applications to folded proteins, *Phys. Rev. E* **83**, 061908 (2011).